Advances in Materials Research, *Vol. 14, No. 3 (2025) 269-282*
https://doi.org/10.12989/amr.2025.14.3.269

Deformation inhomogeneity of the stainless steel – low-carbon steel composite

Svetlana A. Barannikova* and Yulia V. Li

Strength Physics Laboratory, Institute of Strength Physics and Materials Science, Siberian Branch of Russian Academy of Science, Tomsk 634055, Russia

(*Received July 14, 2023, Revised June 20, 2025, Accepted June 26, 2025*)

Abstract. The kinetics of plastic flow localization in low carbon steel/stainless chromium-nickel steel (ASTM A414 grade A / AISI 304) composite under uniaxial tensile testing is studied via digital speckle image correlation method. The types and parameters of local deformation in the base and cladding layers of the composite are determined at different stages of work hardening. It is found that in the low carbon steel basal layer, the distribution of localized deformation at the yield plateau represents a single localized front similar to the Lüders band. In the austenitic steel coating layer, the distribution of localized deformation at the yield plateau represents localized fronts similar to the Portevin–Le Chatelier effect bands.

Keywords: composite; deformation fields; digital image correlation; Lüders band; steel; tensile testing

1. Introduction

The development of modern technology has led to the need to create materials with a complex of properties that provide high strength, corrosion resistance, thermal conductivity, heat resistance, wear resistance, etc. (Pelleg 2013). In this respect, particular attention is paid to composites made by combining two or more dissimilar metals into a monolithic composition that preserves the reliable linking between the constituents during further processing under operating conditions (Xiao *et al*. 2012). There are currently numerous methods to obtain bimetals with various functions and compositions (Li *et al*. 2022), which allow one to take into account the specificities of each type of materials. Many studies have been devoted so far to the mechanical properties of bimetals (Li *et al*. 2020). For instance, the strong junction between metal layers over the entire contact surface is the main purpose in the production of metal composites. At the same time, it is important to achieve the required ratio of layer thicknesses, as well as the structure and properties of the finished composite (Li *et al*. 2018). Moreover, the combination of hard steel with softer one makes it possible to significantly increase the service life of bimetallic products. The effect of heat treatment on the interfacial characteristics, mechanical properties and fracture behavior of a bimetallic composite made of duplex stainless steel 2205 / carbon steel AH36 has been considered in detail in work (Li *et al*. 2020). Heterogeneity of both the microstructure and chemical composition has been observed in the zone adjacent to the interface. It was established that the diffusion transition zone of the Cr and

*Corresponding author, Professor, E-mail: bsa@ispms.ru

http://www.techno-press.org/?journal=amr&subpage=5 ISSN: 2234-0912 (Print), 2234-179X (Online)

Fe alloy elements between the 2205 component and the AH36 steel layers tended to enlarge with an increase in the annealing temperature. The results of shear and tensile tests showed that the tensile strength of the 2205/AH36 bimetallic composite gradually decreased, but the elongation during fracture increased with the rising annealing temperature. Besides that, a wider diffusion zone of alloying elements led to the increase in interfacial shear strength and plasticity of the bimetallic composite. The study (Ea *et al*. 2016) provides deformation field maps under quasi-static and dynamic uniaxial tension of Ti/Al laminated slabs obtained via explosion welding. The energy dispersive spectroscopy and high-resolution synchrotron X-ray diffraction analyses of samples loaded in the directions parallel and perpendicular to the interface enabled one to identify various mechanisms of deformation of layered composites. In particular, it was found that plastic deformation and failure of slabs proceeded mainly in the perpendicularly loaded Al layer. At the same time, for the load applied parallel to the interface, both Ti and Al layers and the interface of the layered material played an important role for plastic flow processes.

At the same time, despite the high strength, bimetallic materials are very sensitive to defects such as "delamination" that emerge at the junction boundary during manufacture and operation, still limiting the widespread use of related products in industry. Besides, the uneven deformation of layered compositions during rolling, depending on various factors (e.g., the ratio of deformation resistances of the components composing the bimetal, the initial thicknesses of the layers and their stacking order, the parameters of the deformation foci, as well as the contact friction forces and tangential stresses at the junction boundaries), has a negative effect on the rolling process and the properties of the bimetal by provoking significant residual stresses that can cause and fracture of monolithic materials (Asaro and Lubarda 2006) and individual components of layered structures (Rizov 2012) fail to directly assess the localization of plastic deformation and cracking within the junction of layers.

During recent decades we have been engaged in research into the macro-scale development of plastic flow. There are two ways to describe strength and plasticity. The first one is based on the theory of defects in the crystal structure (dislocations) (Argon 2008) and the second one uses the methods of mechanics of deformable solids (Han 2005). The corresponding approaches differ mainly in the scale of averaging the properties of the deformable medium. The dislocation approach is microscopic and aims to describe the elementary acts of plasticity, while the mechanical approach is used to establish a functional relationship between the loads applied to the body and the deformations in it, while tending to the macroscopic scale. Unfortunately, these approaches are difficult to reconcile with each other, which prevents the construction of a unified theory of plasticity suitable for all materials. The reason for this situation is the huge difference in the spatial scales of microscopic and macroscopic effects of plasticity.

The inadequacy of traditional approaches initiated the search for new views on the nature of plasticity, which would take into account such important properties of a deformable medium as its multiscale nature (Zaiser 2006).

Dissatisfaction with the possibilities of traditional approaches brought a new paradigm, based on the theory of nonequilibrium systems (Dodd *et al*. 1982). Seeger and Frank (1987) interpreted the response of a medium to a load as a process of its structuring (self-organization). An approach began to be studied in which the evolution of plastic flow was interpreted as a process of self-organization of an ensemble of defects in a crystalline solid.

An important step was the advancement of a hypothesis about the nature of plasticity (Zuev and Barannikova 2019) according to which self-organization of a defective structure of a material takes the form of a macroscale localization of plastic deformation and accompanies the deformation

process from an elastic–plastic transition to failure. Localization acquires in this way different configurations and serves as a source of information about plastic flow.

The validity of the hypothesis was proved in a series of systematic experiments carried out on more than 50 different materials (Zuev and Khon 2022). In their course, it was found that the regions of localized strain during plastic flow self-organize on the sample surface into a specific pattern, the morphology of which carries quantitative information about the kinetics of the spatiotemporal evolution of deformation processes (Scott 2003).

On the basis of the proposed hypothesis about the universality of the macroscale strain localization, the autowave concept of plastic flow of materials was developed (Zuev and Barannikova 2019). Within its framework, it is assumed that the deformation processes in the medium are concentrated in the centers of strain localization, which spontaneously form an ordered evolving deformation structure. This structure exists in the form of autowaves of localized plastic flow, and the pattern is a projection of autowaves onto the surface of a deformable sample.

The fundamental principles of the autowave concept of plastic flow reduce to the experimentally established correspondence rule, which asserts that the autowave modes successively formed in the medium are uniquely associated with the stages of work hardening (Argon 2008), i.e.:

— the stage of the yield plateau (Luders deformation) corresponds to the *switching autowave*;

— a jump-like deformation (the Portevin–Le Chatelier effect) corresponds to an *excitation autowave*;

— at the stage of linear work hardening, a *phase autowave* is formed;

— with parabolic work hardening, a *stationary dissipative structure* arises;

— at the pre-fracture stage, the process ends with the *collapse of the localized flow autowave*.

Thus, in the light of the autowave concept, the process of plastic flow is regarded as a regular change of autowave modes, each of which is controlled by the operation of a specific dislocation strain mechanism that ensures the fulfillment of the law of strain hardening characteristic of a given stage of the plastic flow process (Argon 2008). The correspondence rule provides a predictive capability of the developed autowave model of plasticity. As the experimental analysis of the evolution of the localized plasticity pattern has shown, the rule is fulfilled at any stage of the deformation process and is valid for metals and alloys. This makes the autowave approach to describing the phenomenon of plasticity universal and suitable for explaining the dynamics of deformation of materials, regardless of their nature and structure.

In this regard, it is worth understanding how the localized plastic deformation can develop in a composite material consisting, for example, of metals with various types of plastic flow whereby one component undergoes deformation according to Lüders mechanism, and the other one experiences martensitic transformation. The answer to this question may have a great practical meaning related to pressure-assisted treatment of multilayer structural steel–stainless steel materials used in chemical engineering.

2. Materials and methods

A three-layer composite was produced via cladding with subsequent rolling to achieve the thickness of 8 mm (Barannikova *et al*. 2018). The steel sheet was prepared by hot rolling, from a ingot obtained by the addition of a hot metal (ASTM A414 grade A steel) between two coating AISI 304 steel sheets placed in a mould. The rolling temperature ranged between 1200–1400°C. The cladding layers of AISI 304 austenite stainless steel were 0.75 mm thick and consisted of doped

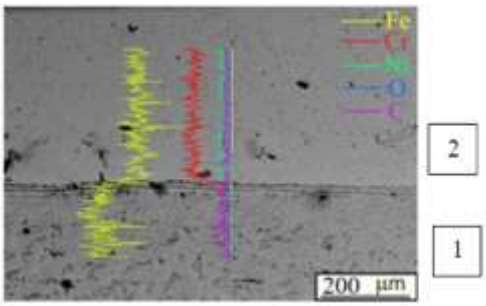

Fig. 1 SEM image and elemental distribution near the interfaces between the base (1) and cladding (2) layers

austenite (γ-Fe, FCC). The base layer of ASTM A414 grade A low-carbon steel with 6.5 mm thick was a quasi-pure ferrite (α-Fe, BCC). Microstructural studies (Fig. 1) were carried out using scanning electron microscope (SEM) LEO EVO-50 (Carl Zeiss, Oberkochen, Germany) with the Oxford Instruments attachment for X-ray dispersion microanalysis. The structure of the cladding metal is typical of stainless steels and reveals austenite grains extended along the rolling direction. The basic metal exhibits the structure typical of low-carbon steels with a ferrite matrix including a small amount of perlite. The microstructure of composite in the junction zone were considered in work (Barannikova *et al*. 2018). The zone of the base metal, consisting of ferrite and pearlite is located at a distance of 2 mm from the interface. A partially decarburized region was observed at a distance of 200 μm from the interface, and a decarburized layer of ferrite, at the interface. Individual inclusions and pearlitic interlayers were observed in the partially decarburized region of the low-carbon steel along ferrite grain boundaries. The cementite of pearlite looks like thin parallel lamellae, alternating with ferritic lamellae. Cementite lamellae are discontinuous; they are curved and different in thickness, which may indicate heterogeneous precipitation of cementite within a single grain. The content of Fe, Cr, Ni and C elements changed near the interfaces between the base and cladding layers due diffusion of elements from stainless steel into low carbon steel. The chromium content in low-carbon steel increases from 0.17 to 0.39 wt % with decreasing distance to the interface. However, the chromium content decreases from 17.15 to 15.5 wt % from the side of the cladding layer (austenitic steel) in the junction region. The carbon content at a distance of 10 μm from the interface increased from initial 0.12 to 0.32 wt % in the austenitic steel. The distribution of elements (Fig. 1) is in agreement with the microhardness distribution over the bimetal thickness.

The microhardness at the interface is much higher than that of the base and the cladding layers. Such a change in the microhardness over the interface width can be explained by the following two competing effects due to directional flows: carbon from the low-carbon steel and alloying elements (Cr and Ni) from the austenitic steel. The first flow causes softening of the material and the formation of a ferritic structure near the interface in the low-carbon, where a pearlite structure initially was observed. The second flow, on the contrary, causes hardening. After the end of the yield plateau, microcracks and martensitic α' - phase were observed in the cladding layer of the stainless steel composite as a result of the γ-α' phase transformation (Shin *et al*. 2001). The amount of α'-martensite phase in the cladding layer of AISI 304 stainless steel in the deformed composite was determined via X-ray diffraction on the DRON-3 installation using monochromatic Cu Kα radiation (Fig. 2). The XRD analysis of the surface layer of AISI 304 steel in the composite showed that the initial structure contained only austenite (γ-phase) with a lattice parameter a = 3.5999 Å. In turn, a deformation-induced γ-α'-phase transformation was realized in tensile-deformed surface layers of

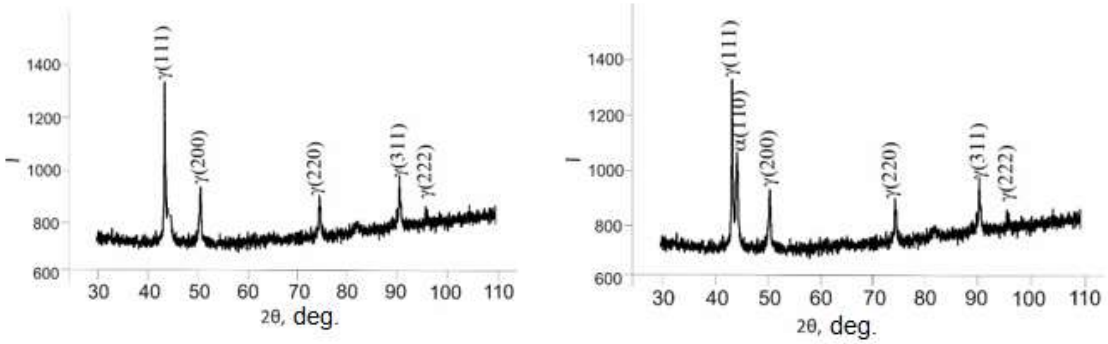

(a) The non-deformed state (b) The yield plateau

Fig. 2 X-ray diffraction patterns for the cladding layer

AISI 304 stainless steel (Shin *et al*. 2001), and a two-phase structure with different ratios of *α'*- and *γ*-phases was revealed. Austenitic steel AISI 304 has an unstable structure in which phase transformations with the formation of α'-phase particles can occur under the applied load (Shin *et al*. 2001). The features of localized plastic flow in metastable austenitic steels under tensile testing were investigated in study (Barannikova and Iskhakova 2022).

The composite samples were cut so that the base and cladding layers could be seen on the observation surface. The samples had the dimensions of 42×8×2 mm and were loaded at 300 K at a rate of $\sim 8 \cdot 10^{-5}$ s^{-1} on a Walter Bai AG LFM-125 testing machine. The stress-strain curve of the composite included the regions of elastic and plastic strains and failure. The composite plastic strain curve located between two curves of its components (Barannikova *et al*. 2018). Similarto the ASTM A414 grade A specimen, the stress-strain curves of the AISI 304 specimen showed the peak and the yield plateau, both appeared prior to those in the ASTM A414 grade A specimen.

The mechanical properties of the three-layer composite differed from that of its components (Table 1). The yield point of the composite approached to the yield point of the ASTM A414 grade A specimen, whereas the yield point of the AISI 304 specimen was higher than in the ASTM A414 grade A, but two times lower than in the AISI 304 specimen. The evolution of macroscopically localized plastic flow bands was visualized and monitored via the digital speckle image correlation technique (Zuev and Barannikova 2019). The digital speckle image correlation consists in high-accuracy determination of displacement fields by tracking the surface changes and comparing digital images acquired during uniaxial tensile. This technique is intended for local rate estimation for laser speckle patterns by implying first-order statistics (Welford 1975). The physical basis of the proposed technique and its implementation are described for the case of diffuse object in the work (Ohtsubo and Asakura 1976). On the basis of speckle field statistics (Ohtsubo and Asakura 1976), the motion rate of the point is inversely proportional to the mean-square dispersion of brightness and is directly proportional to the mean brightness squared for the measured point in the time period. Plastic deformation investigations are carried out for metals and alloys using nontransparent samples; therefore, we examined the statistics of speckle patterns on the sample surface. An analysis of the speckle patterns observed experimentally for such diffuse scattering objects suggests that the rate measured for a point on the sample surface is directly proportional to the dispersion of brightness in the time interval. In plastic deformation investigations an analysis of first-order statistics may be supplemented by the application of the conventional speckle photography technique (Jones and

Table 1 Mechanical properties of metals

Material	Yield Strength, MPa	Ultimate Tensile Strength, MPa	Total Elongation, %
Low-carbon Steel ASTM A414 Grade A	255±3	380±4	31±1
300	0.21		
Stainless Steel AISI 304	216±4	730±3	70±2

Wykes 1983); then both sets of data on local strain fields could be matched. To this end, the opposite side of the sample placed in the clamps of the testing machine is illuminated by the coherent light and its speckle photographs are obtained as well.

The decoding procedure of speckle photographs is as follows. First, the tilt and step of the Young bands is determined for pre-assigned points of specklograms, and displacement vector fields ***r****(x, y)* during deformation of flat samples are calculated for the following plastic distortion tensor components:

$$\beta_{ij} = \nabla r(x,y) = \begin{vmatrix} \varepsilon_{xx} & \varepsilon_{xy} \\ \varepsilon_{yx} & \varepsilon_{yy} \end{vmatrix} + \omega_z \tag{1}$$

where

$$\begin{vmatrix} \varepsilon_{xx} & \varepsilon_{xy} \\ \varepsilon_{yx} & \varepsilon_{yy} \end{vmatrix} \equiv \varepsilon_{ij} \tag{2}$$

is the plastic strain tensor and ω_z is the rotation about the z axis. The components of tensor (1)

$$\varepsilon_{xx} = \frac{\partial u}{\partial x},\ \varepsilon_{yy} = \frac{\partial v}{\partial y},\ \varepsilon_{xy} = \frac{1}{2}\left(\frac{\partial v}{\partial x} + \frac{\partial u}{\partial y}\right) = \varepsilon_{yx},\quad \omega_z = \frac{1}{2}\left(\frac{\partial v}{\partial x} - \frac{\partial u}{\partial y}\right) \tag{3}$$

are, respectively, the local tension, narrowing, displacement, and rotation; $u=r\cos\phi$ and $v=r\sin\phi$ are, respectively, the longitudinal and transverse components of the displacement vector **r**; and ϕ is the angle between the vector **r** and tension axis direction.

Numerical operations of smoothing, missing data reconstruction, and differentiation were performed using the RED32 program. Differentiation was carried out over five points of the dependences $u(x)$, $u(y)$, $v(x)$, and $v(y)$, followed by cubic spline interpolation.

The program creates data files $\varepsilon_{xx}(x, y)$, $\varepsilon_{yy}(x, y)$, $\varepsilon_{xy}(x, y)$, $\omega_z(x, y)$ and graphically represents the results in the form of displacement vector fields **r**(x, y), transformation patterns of rectangular meshes on the sample surface or the distributions of distortion tensor components (1) over the sample. Then, quantitative data on the kinetics of the development of plastic flow localization are obtained from the time dependences of coordinates X of localization nuclei, i.e., curves $X(t)$. Thus, we can determine the spatial λ and temporal T periods of the corresponding distributions and the nucleus motion velocity $V_{aw}=\lambda/T$.

In this work, the deformable sample was illuminated by a coherent beam of a semiconductor laser with a wavelength of 635 nm and a power of 15 W. The images of the deformable sample with the superposed speckle structures were recorded using a Pixellink PL-B781 digital video camera with a frequency of 10 Hz, then digitized and stored as files.

The details and possibilities of the approach are described in work (Zuev *et al*. 2002). The most common tensor component for visualization and analysis is that associated with local elongation in the direction of the extension axis of the sample, i.e., the ε_{xx} component. The distributions of shear

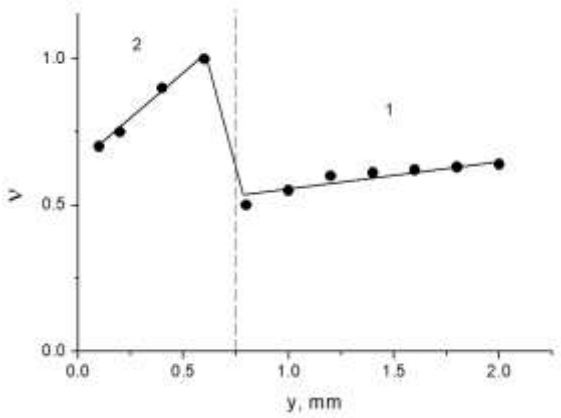

Fig. 3 Change in the coefficient of variation ν of local elongations ε_{xx} by composite thickness for total deformation 0.01. The dotted lines denote the interfaces between the base (1) and cladding (2) layers

and rotary components have usually more complex forms, which make them less convenient for analysis. The degree of plastic deformation inhomogeneity of different layers was quantitatively assessed using the coefficient of variation ν of local strains ε_{xx} as a ratio of the standard deviation to the mean of measurements.

It is assumed that the distribution along the elongation axis $\varepsilon_{xx}(x_i)$ at $\nu > 0.4$ becomes strongly inhomogeneous and the magnitude $<\varepsilon_{xx}>$ is no longer representative (Mendenhall and Sincich, 2016). Fig. 3 displays the distribution in plastic deformation inhomogeneity ν near interface between the base and cladding layers of composite at the initial stages of plastic flow. In the composite after rolling, the difference between the deformation inhomogeneities within the micro-volumes of the border zones near stainless and carbon steels was almost two times. The presence of a carbide interlayer led to an inhomogeneous distribution of local deformations and the crack initiation in the carbonized layer of austenitic steel with a total deformation of 0.01.

3. Experimental results and discussion

In general, the stress-strain diagram of the composite inherits the features characteristic of the deformation of the low-carbon steel base layer, containing a yield plateau and the stages of parabolic work hardening and pre-failure. Moreover, the composite exhibits certain deformation peculiarities in comparison with the individual α-Fe and γ-Fe components, which have been studied earlier (Barannikova and Iskhakova 2022). A solitary focus of local elongations ε_{xx} was observed in the base layer of the composite at the yield plateau with a total deformation of $\varepsilon_{tot} = 0.006$, while no localization foci were detected in the cladding layer. This fact indicated that macroscopically localized plastic flow in the form of Lüders bands emerged in the base layer at the initial stage of deformation earlier than in the cladding layer. At the deformation of $\varepsilon_{tot} = 0.007$, the maximum of local elongations ε_{xx}, corresponding to the localization front, appeared in the cladding layer once the nuclei of the Lüders front inthe base layer reached the junction with the cladding layer. At this moment, the Lüders fronts of the cladding and base layers began to move as a whole toward the grips of the test machine (Fig. 4). According to the local deformation distribution patterns, a single

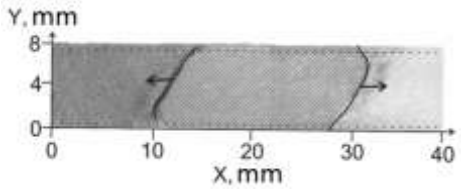

Fig. 4 Halftone picture of distribution of local elongations ε_{xx} on the working part of the sample. Arrows indicate the direction of movement of the Lüders band fronts at the yield plateau. The dotted lines denote the interfaces between the base and cladding layers

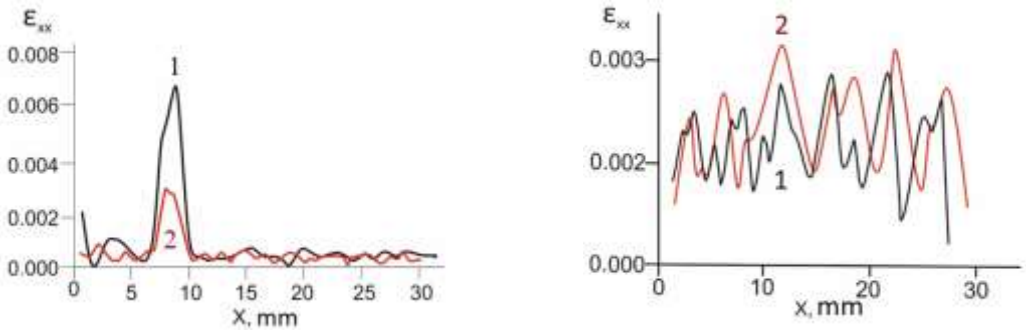

(a) The yield plateau (b) The parabolic work hardening stage

Fig. 5 Distributions of local elongations ε_{xx} along the tensile axis of the composite: 1 – base layer of low-carbon steel; 2 – cladding layer of austenitic stainless steel

Lüders front arose in the base layer near the junction at the earlier stages of plastic flow, which then initiated the nucleation of the front in the cladding layer. At the yield point, the singular front propagated in both the base and cladding layers, which is usually untypical at the beginning of plastic deformation (Fig. 5 a).

The distributions obtained in this way reflect the increments of local deformations rather than their integral values from the beginning of the loading process. It is worth noting that Lüders fronts are characteristic of low-carbon steels at the yield plateau (Srinivasan *et al*. 2012). In austenitic steels, the formation of singular localized deformation fronts (Lüders fronts) within the earlier stages of plastic flow at room temperature has not been observed so far.

However, the Portevin–Le Chatelier (PLC) effect was investigated in a metastable austenitic CrMnNi cast steel during tensile tests for the wide range of deformation temperatures and nominal strain rates (Möller *et al*. 2016). Analysis of the stress–strain curves was complemented by in situ measurements of thermal and acoustic emissions as well as by digital image correlation, enabling determination of various local characteristics of plastic flow and clarification of individual contributions of different micro-scopic mechanisms involved in plastic deformation. It was shown that the PLC effect in the investigated CrMnNi steel was caused by the diffusion of interstitial atoms in the bcc phases (deformation-induced α'- martensite) (Möller *et al*. 2016). The most commonly accepted explanation for the origin of the PLC effect is based on a dynamic strain-aging model associated with the interaction between the motion of mobile dislocations and the diffusion of interstitials like carbon toward the dislocation cores (Yilmaz 2011). The motion of dislocations is impeded by the segregation of solute interstitials along the dislocation line, thus promoting repeating dislocation avalanches due to unpinning from solutes with the increasing strain (Dierke *et al*. 2011).

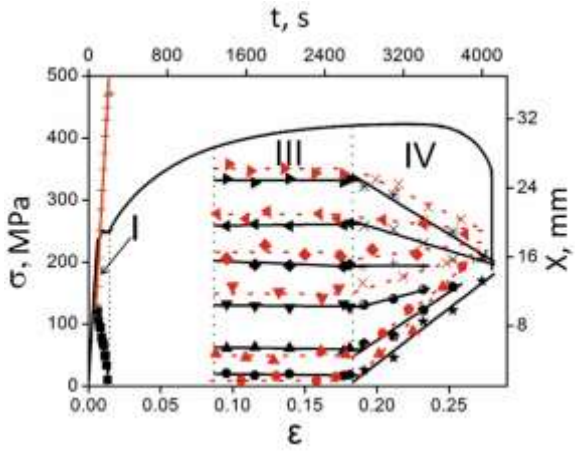

Fig. 6 Kinetic *X*-*t* diagrams of spatio-temporary evolution of localized deformation fronts in the composite: I – yield plateau; III – parabolic work hardening stage; IV – pre-failure. Solid lines – base layer; dotted lines – cladding layer

Accordingly, a change from spatially homogeneous and temporarily steady to inhomogeneous and unstable deformation occurs. As a result, strain localization is observed in the form of macroscopic bands with thicknesses of a few millimeters—the so-called PLC bands—which emerge and propagate along the gauge length, causing significant surface roughening (Müller *et al*. 2016).

One important characteristic of localized plastic flow is the velocity of the localized deformation front, which can be determined from the *X*-*t* diagrams in Fig. 6, where the points indicate the positions of the maximal local elongations ε_{xx} along the *X* axis of the sample at the loading time *t*. At the yield plateau (Fig. 6, stage I), the Lüders fronts emerging in the base layer moved in opposite directions at the speeds of $1.5 \cdot 10^{-4}$ m/s and $1.2 \cdot 10^{-4}$ m/s. In the composite, two fronts propagated in opposite directions in the cladding layer with the velocities of $0.7 \cdot 10^{-4}$ m/s and $2.3 \cdot 10^{-4}$ m/s (Fig. 6, stage I). The analysis of the propagation velocities of localized deformation fronts in the base and cladding layers with the corresponding values for monolithic samples of ASTM A414 grade A carbon steel and AISI 304 austenitic steel revealed that the 0.75 mm thick cladding layer did not suppress the formation of Lüders bands. On the contrary, the propagation velocities of Lüders fronts in the base and cladding layers were increased compared with the individual components of the composite. Furthermore, a series of equidistant foci of localized plastic flow with a characteristic distance of 4±1 mm between them were observed at the stage of parabolic work hardening in the base and cladding layers (Fig. 5b). With an increase in the total deformation, those foci remained steady and represented a stationary dissipative structure (Fig. 6, stage III). At the pre-failure stage of the composite, the initially stationary foci of plastic deformation localization in the γ-Fe and α-Fe layers began to move at different speeds toward the high-amplitude maximum of local deformations (the neck nucleation site) (Fig. 6, stage IV).

The study of the failure stage of the composite under uniaxial tensile revealed that failure was initiated with the emergence of a stress concentration in the form of a crack in the cladding layer, which then propagated in the base layer (Fig. 7). The crack formed in the cladding layer then grew in the base layer and was divided into numerous small cracks while moved, thereby reducing the speed of its propagation. As soon as the crack passed through the entire cross-section of the sample,

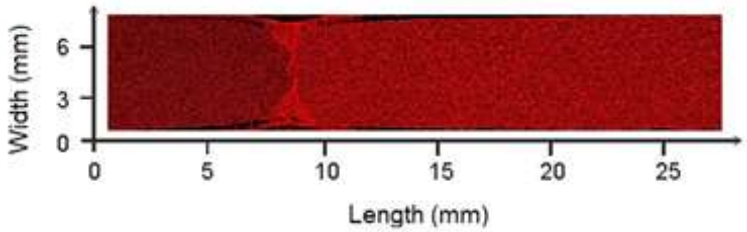

Fig. 7 Localized deformation pattern for pre- failure stage

the latter underwent failure. The above-described phenomena exhibit significant differences in the character of the development of the localized deformation, which primarily concern the kinetics of the development of the localization patterns. In the case of the expansion of a Lüders band in the limits of the gage part of the sample, plastic deformation is localized in the regions of fronts moving in opposite directions that have complex shapes that change in the process of motion. Upon the motion of the fronts, the rule of the constancy of the sum of the moduli of their velocities is fulfilled. If two Lüders bands are expanded in the sample simultaneously, the meeting and the interaction of the fronts can occur, which is usually reduced to the mutual extinction of plastic deformation and the local disappearance of the fronts.

Upon deformation, the fronts of the Lüders band can travel along the sample only one time. In the case of the Portevin–Le Chatelier effect, the zone of plastic deformation develops such that, at each time moment, there is only one narrow moving band in which the plastic flow is completely localized. These bands repeatedly pass along the gage part of the sample (Manach, 2014).

At the pre-failure stage, the zones of localized deformation move upon the formation of the neck preceding the ductile failure in such a manner that the rectilinear graphs of the time dependence of their positions $X(t)$ converge at one point (Fig. 6). The zone of plastic flow eventually narrows, degenerating into the surface of a viscous crack. The comparison of the results obtained leads to the conclusion that the observed variants of the development of the macroscopic localization of plastic flow in the investigated cases can be reduced to a simple kinematic scheme, in which the width of the active zone of plastic deformation behaves as follows:

- it grows following the Luders deformation;
- it remains constant in the case of the Portevin–Le Chatelier effect;
- it becomes narrower following the formation of a neck in the sample.

These kinematic differences are connected with the different nature of the micro-mechanisms of the deformation of each of the observed phenomena, i.e., by the specific microstructure of the active medium subjected to deformation, which provides the opportunity to generate autowaves of the localized plasticity in open systems (Scott, 2003).

It is noteworthy that though austenitic steel has a high level of strength and plasticity in the monolithic state (Table 1), the plastic flow localization and accumulation of microcracks in the three-layer composite occur faster than in the base layer of low-carbon steel. To explain the mechanisms of localized plasticity in the cladding layer and the failure of the composite, the Lüders front in the base layer was assumed to wedge the material and initiate the cracking in the cladding layer once meeting the interface in the composite (Fig. 8).

The size of the equilibrium crack in front of the wedge can be determined using the model proposed by Barenblatt (1959) as follows:

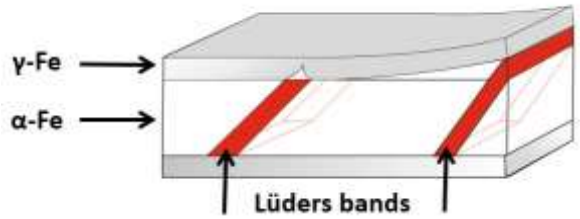

Fig. 8 Schematic of layer wedging in the composite

$$l^* = \frac{E^2 h^2}{4K_I^2(1-\mu^2)^2} \tag{3}$$

where h is the width of the wedge, E is the elastic modulus, μ is the Poisson's ratio, and K_1 is the fracture toughness characterizing the force of interaction between the walls of the crack near its end (a constant value).

Assuming that $E = 2 \cdot 10^{-5}$ MPa; $h \approx 10^{-4}$ m is the width of the Lüders front in the base layer; $\mu = 0.3$; $K_1 = 2.5 \cdot 10^3$ MPa·m$^{1/2}$ is the coupling modulus for α-Fe phase, the length of the crack formed in front of the wedge in the cladding layer will be equal to $l^* \approx 20$ μm. Since the microscopic analysis revealed cracks in the cladding layer with a length of $l \approx 30 \pm 7$ μm, it can be stated with certainty that the wedging force of the Lüders bands growing in the base layer has created a microcrack as long as several tens of micrometers, the elastic field of which induced the local stress concentration in the cladding layer.

The local stresses σ_c of crack nucleation can be estimated in accordance with the Griffiths equation (Broek 1986) as follows:

$$\sigma_c = \left(\frac{E\gamma}{2\pi l^*}\right)^{1/2} \tag{4}$$

where γ is the surface energy density. Then, at the crack length of $l^* \approx 30$ μm in the cladding layer near the junction in AISI 304 steel, a critical local stress is $\sigma_c = 4460$ MPa. In other words, the condition for crack initiation in the cladding layer of stainless steel is fulfilled when the stress reaches a critical value conforming to the strength criterion of failure. However, there is no failure of the bimetal at the end of the yield plateau, mainly because the crack propagation in the composite is inhibited by the interface. In this case, the stress σ_c relaxes with the formation of localized plasticity fronts.

The mechanism of plastic deformation in the cladding layer of the composite was considered by Barannikova and Li (2020). Specifically, it was shown that the high local stress at the interface between the base and cladding layers of the composite induced the formation of the martensitic α'-phase (Shin *et al*. 2001) and thereby triggered the nucleation of the Portevin-Le Chatelier bands (Hähner 1994) in the AISI 304 cladding layer. Such bands were fixed at the later stage of intermittent flow during tensile of monolithic austenitic steel samples at plastic flow stresses of ~700 MPa (Barannikova and Iskhakova 2022). This suggests that when the composite is deformed at the yield plateau in the cladding and base layers, there is not a single Lüders band but two different bands of localized plastic flow, that is, the Lüders band in α-Fe and the Portevin-Le Chatelier band in γ-Fe, respectively.

4. Conclusions

Based on the method of the digital speckle image correlation and tracking of speckle pattern, the macroscopic localized plastic strain was investigated in the real time conditions, under the composite uniaxial tension, that allowed us to determine the localized strain distribution in different composite layers such as low-carbon steel and austenitic stainless steel.

• The study of the low carbon steel–stainless steel composite revealed that localized plasticity fronts formed and evolved in a regular way in the base and cladding layers throughout the plastic flow.

• At the yield plateau, the Lüders band took its origin from the inner cladding–base metal interface. When passing through the entire cross-section of the base layer, the elastic field of the Lüders band induced the local stress concentration in the cladding layer and triggered the Portevin-Le Chatelier effect.

• At the stage of parabolic work hardening, the joint deformation of the base and cladding layers was accompanied by a stationary pattern of localized plastic flow foci.

• The failure of the composite began with the crack nucleation in the cladding layers of the composite, which then spread in the base layer.

Based on the findings of the current study, some recommendations concerning the effective development of cold rolling technology of low carbon steel/stainless chromium-nickel steel bimetals can be made. One of the main issues to be solved is associated with the maximum possible reduction in the course of one or more passes that would cause neither continuity violations nor failure of the material. Such reduction is usually established empirically on the basis of laborious and expensive production tests. However, if the limits of macroscopically uniform deformation are known, then the degree of reduction must suit them. According to the above results, these are the sections of the stress-strain curves, corresponding to chaotically localized plastic flow patterns or moving deformation foci. In the latter case, even though the plastic flow is localized at each specific moment of time, it exhibits a quasi-uniform process during the loading.

Thus, preference should be given to reduction within the linear work hardening and the parabolic work hardening stage with a low parabolicity index. Plastic flow localization at the parabolic work hardening stage is a stationary process, but there are still many localization zones without internal continuity disturbances (microcracks). Therefore, reduction at the beginning of the parabolic work hardening stage is also acceptable. The only exception is the modes with stationary single zones of plastic flow localization, which are technologically unacceptable and even dangerous (Zuev *et al*. 2020).

The analysis of the plasticity during pressure-assisted treatment cannot be limited to only the assessment of traditional indicators (strength stress and elongation at break), but should include a thorough study of the patterns of macroscopically localized plastic flow (Zuev and Barannikova, 2019). Plastic deformation of the composite facilitates diffusion processes. When diffusing dissimilar steels, taking into account their physical and chemical properties, strength requirements, permissible level of plastic deformation of parts and the need for subsequent thermo-mechanical treatment, it is necessary to select a technology using an intermediate layer in the form of a diffusion barrier applied to the surface of austenitic steel before joint rolling.

Joining metals through an intermediate layer will avoid macroscopic localization of deformation in the contact area. These recommendations can be useful, for example, when optimizing the manufacture technology of industrial products made of low carbon steel/stainless chromium-nickel steel composite (pipes, pressure vessels, etc.).

Acknowledgments

The authors thank Prof. L.B. Zuev for advice and helpful discussion. This research was carried out using the equipment of the Central Research Center "Nanotech" of the Institute of Strength Physics and Materials Science, Siberian Branch of the Russian Academy of Sciences.

Funding

This study was carried out within the frames of the Governmental Assignment for ISPMS SB RAS, project No. FWRW-2021-0011.

References

Argon, A. (2008), *Strengthening Mechanism of Crystal Plasticity*, University Press, Oxford, U.K.

Asaro, R.J. and Lubarda, V.A. (2006), *Mechanics of Solid Materials*, Cambridge University Press, Cambridge, U.K.

Barannikova, S.A. and Iskhakova, P.V. (2022), "Study of deformation structures maps in metals under tension", *PNRPU Mech. Bull.*, **3**, 107-115. https://doi.org/10.15593/perm.mech/2022.3.11

Barannikova, S.A. and Li, Y.V. (2020), "Development Kinetics of the Plastic Wave Front at the Metal Interface", *Russ. Phys. J.*, **63**, 731-737. https://doi.org/10.1007/s11182-020-02091-7

Barannikova, S., Zuev, L. and Li, Y. (2018) "Plastic flow heterogeneity and failure of bimetal material", *Int. J. Geomate*, **14**, 112-117. https://doi.org/10.21660/2018.43.3578

Barenblatt, G.I. (1959), "The formation of equilibrium cracks during brittle fracture. General ideas and hypotheses. Axially-symmetric cracks", *J. Appl. Math. Mech.*, **23**, 622-636. https://doi.org/10.1016/0021-8928(59)90157-1

Broek, D. (1986), *Elementary Engineering Fracture Mechanics*, Marinus Nijhoff Publishers, Dordrecht, Germany. https://doi.org/10.1007/978-94-009-4333-9

Dierke, H., Fischer, M., Tutsch, R. and Casarotto, L. (2011), "Optical Extensometer for Tracking Propagations Deformation Bands", *Tech. Mess.*, **78**, 211-217. https://doi.org/10.1524/teme.2011.0106

Dodd, R.K., Eilbeck, J.C., Gibbon, J.D., Morris, H.C. (1982), *Solitons and Nonlinear Wave Equations*, Academic Press, London, U.K.

E, J.C., Huang, J.Y., Bie, B.X., Sun, T., Fezzaa, K., Xiao, X.H., Sun, W. and Luo, S.N. (2016), "Deformation and fracture of explosion-welded Ti/Al plates: A synchrotron-based study", *Mater. Sci. Eng. A*, **674**, 308-317. https://doi.org/10.1016/j.msea.2016.07.125.

Han, C.W. (2005), *Continuum Mechanics and Plasticity*. Chapmen and Hall, New York, U.S.A.

Hähner, P. (1994), "Theory of solitary plastic waves", *J. Appl. Phys. A*, **58**, 41-58. https://doi.org/10.1007/BF00331516

Jones, R. and Wykes, C. (1983), *Holographic and Speckle Interferometry*, Cambridge University Press, Cambridge, U.K.

Li, Y., Gong, M., Wang, K., Li, P., Yang, X. and Tong, W. (2018), "Diffusion behavior and mechanical properties of high chromium cast iron/low carbon steel bimetal", *Mater. Sci. Eng. A*, **718**, 260-266. https://doi.org/10.1016/j.msea.2018.01.111

Li, Z., Lin, Y.C., Zhang, L., Jiang, F., Jiang, Z. and Jiao, S. (2022), "Investigation of compact tensile and fracture mechanical properties of a duplex stainless steel bimetal composite with the interfacial zone", *J. Mater. Res. Tech.*, **19**, 809-820. https://doi.org/10.1016/j.jmrt.2022.05.085

Li, Z., Zhao, J., Jiang, F., Liang, X., Zhang, Q., Yuan, X., Jiao, S. and Jiang, Z. (2020) "Interfacial characteristics and mechanical properties of duplex stainless steel bimetal composite by heat treatment",

Mater. Sci. Eng. A, **787**, 139513, 1-24. http://doi.org/10.1016/j.msea.2020.139513
Manach, P.Y., Thuillier, S., Yoon, J.W., Coer, J. and Laurent, H. (2014) "Kinematics of Portevin–le Chatelier bands in simple shear", *Int. J. Plast.*, **58**, 66-83. http://doi.org/10.1016/j.ijplas.2014.02.005
Mendenhall, W.M. and Sincich, T.L. (2016), *Statistics for Engineering and the Sciences*, Chapman and Hall/CRC, New York, U.S.A.
Müller, A., Segel, C., Linderov, M., Vinogradov, A., Weidner, A. and Biermann, H. (2016), *"*The Portevin–Le Châtelier Effect in a metastable austenitic stainless steel", *Metall. Mater. Trans. A.*, **47**, 59-74. https://doi.org/10.1007/s11661-015-2953-x
Ohtsubo, J. and Asakura, T. (1976), "Velocity measurement of a diffuse object by using time-varying speckles", *Opt. Quantum Electron.*, **8,** 523-529. https://doi.org/10.1007/BF00620143
Pelleg, J. (2013), *Mechanical Properties of Materials*, Springer, Dordrecht, Germany. https://doi.org/10.1007/978-94-007-4342-7
Rizov, V. (2012), "Fracture in Composites - An Overview (Part I)", *J. Theor. Appl. Mech.*, **42**, 3-42. https://doi.org/10.2478/v10254-012-0006-z
Scott, A. (2003), *Nonlinear Science, Emergence and Dynamics of Coherent Structures*, University Press, Oxford, U.K.
Seeger, A. and Frank, W. (1987), "Structure formation by dissipative processes in crystals with high defect densities", *Nonlinear Phenomena Mater. Sci. Trans. Tech.*, 125-138, New York, U.S.A.
Shin, H.C., Ha, T.K. and Chang, Y.W. (2001), "Kinetics of deformation induced martensitic transformation in a 304 stainless steel", *Scripta Mater.*, **45** (7), 823-829. https://doi.org 10.1016/S1359-6462(01)01101-0
Srinivasan, N., Raghu, N. and Venkatraman, B. (2012), "Study on Lüders deformation in welded mild steel using infrared thermography and digital image correlation", *Adv. Mater. Res.*, **585**, 82-86. https://doi.org/10.4028/www.scientific.net/AMR.585.82
Welford, W.T. (1975), "First order statistics of speckle produced by weak scattering media", *Opt. Quantum Electron.*, **7**, 413-416. https://doi.org/10.1007/BF00619839
Xiao, X.F., Ye, S.P., Yin, W.X. and Xue, Q. (2012), "HCWCI/Carbon steel bimetal liner by liquid-liquid compound lost foam casting", *J. Iron Steel Res.*, **19**, 13-19. https://doi.org/10.1016/S1006-706X(12)60145-9
Yilmaz, A. (2011), "The Portevin–Le Chatelier effect: a review of experimental findings", *Sci. Tech. Adv. Mater.*, **12**, 1-16. https://doi.org/10.1088/1468-6996/12/6/063001
Zaiser, M. (2006), "Scale invariance in plastic flow of crystalline solids", *Adv. Phys.* **5**, 185-245. https://doi.org/10.1080/00018730600583514
Zuev, L.B., Polyakov, S.N. and Gorbatenko, V.V. (2002), "Instrumentation for speckle interferometry and techniques for investigating deformation and fracture", *Proc. SPIE*, **4900**, 1197-1208. https://doi.org/10.1117/12.484526
Zuev, L.B. and Barannikova, S.A. (2019), "Autowave physics of material plasticity", *Cryst.*, **9**, 458-488. https://doi.org/10.3390/cryst9090458
Zuev, L.B., Shlyakhova, G.V. and Barannikova, S.A. (2020), "Effect of Radial Forging on the Microstructure and Mechanical Properties of Ti-Based Alloys", *Metals*, **10**, 1488. https://doi.org/10.3390/met10111488
Zuev, L.B. and Khon, Y.A. (2022), "Plastic flow as spatiotemporal structure formation, Part I, Qualitative and quantitative patterns", *Phys. Mesomech.*, **25**, 103-110. https://doi.org/10.1134/S1029959922020011

CC